Analysis of Failure Sources in Surface-Micromachined MEMS*

N. Deb and *R. D. (Shawn) Blanton*
Center for Electronic Design Automation
Department of Electrical and Computer Engineering
Carnegie Mellon University
Pittsburgh, PA 15213
email: {ndeb, blanton}@ece.cmu.edu

Abstract

The effect of vertical stiction, foreign particles, and etch variation on the resonant frequency of a surface-micromachined resonator and accelerometer are presented. For each device, it is shown that misbehaviors resulting from different failure sources can overlap, exhibit dominance and combine to create behavior masking and construction. Such an analysis is essential for developing test and diagnosis methodologies for surface-micromachined MEMS.

1 Introduction

MicroElectroMechanical Systems (MEMS) are a multi-domain discipline whose heterogeneity results from the use of interacting mechanical and electronic devices. With the emergence of stable process technologies, the focus is now on the design of systems containing hundreds or even thousands of mixed-domain components. CAD tools that shorten the design and development time for MEMS-based products [1] are therefore increasingly needed. In addition, robust fault models and test methods are required to ensure high yield and reliability of MEMS products, especially for the many life-critical applications involving MEMS such as air-bags and bio-sensors.

Surface-micromachined MEMS devices contain micromechanical structures that are fabricated using layers of thin films deposited on the substrate. Surface micromachining enables the fabrication of high-quality MEMS devices. Most commercial applications use surface micromachining because of its well-developed infrastructure for depositing, patterning and etching of thin films for silicon integrated circuits. Early applications of this technology include the digital mirror display [2] and the accelerometer [3]. These industrial successes and the open availability of processes such as MUMPS [4] makes surface micromachining a good choice for MEMS test development.

MEMS manufacturing test is the process of screening good devices from a group of fabricated devices. The normal assumption is that the design is correct and that test is the process of verifying that the fabricated device is equivalent to the design. Past work in MEMS test includes behavior-level fault simulation [5, 6], design for manufacturability [7], failure analysis based on process simulation [8], and various defect modeling and classification techniques [9, 10]. Previous work in defect modeling has dealt with failure sources individually. However, an industrially-fabricated MEMS device is likely to be affected by two or more failure sources simultaneously. Hence, there is a need to study the behavior of MEMS under the combined influence of two or more failure sources.

Our work here analyzes the misbehavior of MEMS devices under the influence of various failure sources. A *failure source* is any abnormality in the fabrication process that causes a *defect*, where a defect is any physical (structural or material) change from the intended design. A defect causes *misbehavior* if one or more performance specifications of the defective device fall outside of the specified acceptable range. Failure sources for MEMS include foreign particles, etch variations, and stiction [10], each of which can lead to a variety of defects. For example, in [8] it is shown that particles can lead to defects that include broken and bridged structures with corresponding behaviors that range between benign and catastrophic. We initially analyze the effects of each failure source in isolation and then investigate the impact of realistic combinations of failure sources. The failure sources considered include foreign particles that can be introduced at any step in the fabrication process and at any location within the device layout; process-etch variations that result in device area being altered; and vertical stiction where mechanical structures become permanently fixed to the substrate. The MEMS devices used here represent the most common actuator and sensor structures:

*This research is sponsored by the National Science Foundation under grant MIP-9702678, the Defense Research Projects Agency under Rome Laboratory, Air Force Materiel Command, USAF, under grant F30602-97-2-0323, and the Pennsylvania Infrastructure Technology Alliance.

0-7803-6546-1/00 $10.00 © 2000 IEEE

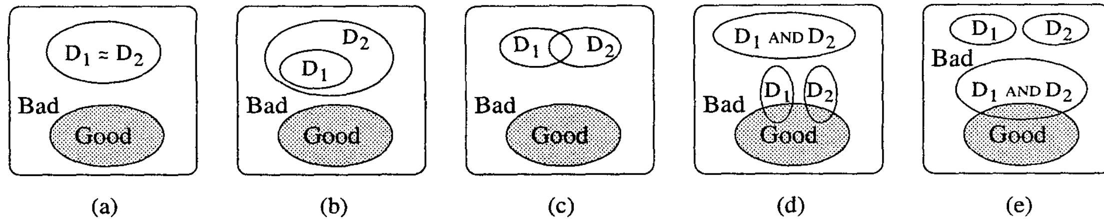

Figure 1: Defect behavior relationships: (a) Misbehavior associated with defects D_1 and D_2 are (virtually) *equivalent*; (b) Misbehavior due to defect D_2 *dominates* that due to defect D_1; (c) Misbehaviors due to defects D_1 and D_2 have a common region and therefore *overlap*; (d) Defects D_1 and D_2 combine *constructively* to produce misbehaviors that are more harmful than the misbehaviors caused by each separately; and (e) Defects D_1 and D_2 combine *destructively* to produce behaviors that are less harmful than the misbehaviors caused by each separately and therefore lead to misbehavior *masking*. Note that the area labeled "Good" is defined as all performance specifications of the device being within the specified acceptable range.

(1) The folded-flexure, electrostatic comb-drive micromechanical resonator introduced by Tang *et al.* [11], and
(2) the standard U-spring, electrostatic comb-drive, single-axis, micromechanical accelerometer [3].

Like electronic circuits, the misbehavior of different failure sources acting in isolation on a MEMS device can be very similar, a situation that obviously hinders diagnosis. Similar misbehaviors caused by different failure sources are cases of misbehavior *overlap*. Also the presence of multiple failure sources may reinforce or cancel effects to cause *constructive* and *destructive* combinations, respectively. A destructive combination is also known as *masking*. Figure 1 illustrates some of the behavioral relationships that can occur between two different defects. While exact behavior *equivalence* is highly unlikely due to the continuous nature of MEMS, the occurrence of behavior *dominance*, *overlap*, *construction*, and *masking* is widespread and will be highlighted with examples.

The organization of the rest of the paper is as follows. Section 2 describes the characteristics of the surface-micromachined resonator, accelerometer, and their respective sources of failure. Sections 3 and 4 discuss the finite element analysis (FEA) predictions of the effect of stiction, etch variation, and particulate contaminations on a resonator and accelerometer structure, respectively. Specifically, FEA is used to analyze the impact of these failure sources on a key performance specification of these devices. Section 5 draws conclusions and describes directions for future work.

2 Surface-Micromachined Devices

We chose the MUMPS (Multi User MEMS Process Service) surface-micromachining technology for our current work [4]. Other surface-micromachining processes are also available from Sandia National Labs [12] and Analog Devices' iMEMS process [13].

2.1 Resonator Actuator

A simplified top-view of the microresonator is shown in Figure 2a, while a representative cross-section is shown in Figure 2b. This device has been extensively studied and is commonly used for MEMS process characterization. Like most MEMS devices, the resonator consists of basic MEMS primitives [1], such as air-gaps, beams, anchors and plates. Primitives are used to make a component and components are used to make a MEMS device. The resonator is a MEMS actuator device made of three major components: a comb-drive, a folded-flexure spring, and a shuttle mass. The movable shuttle mass and the attached comb-fingers are suspended by folded-flexure springs on either side. The other ends of the folded-flexure springs are anchored to the lower layer only at the locations shown. The microresonator can be viewed as a spring-mass-damper system, where the damping is caused by the air surrounding the movable parts, which include the shuttle mass, movable comb-fingers, and spring beams. By applying a voltage across the fixed and movable comb-fingers of the upper comb-drive, an electrostatic force of attraction is produced. The force is directly proportional to the square of the applied voltage. Since every movable finger is located exactly midway between two fixed fingers, the y-component of the electrostatic force is zero and the net force is in the x-direction only. The net force causes the mass to move in the x-direction. The spring suspension, which is designed to be compliant in the x-direction of motion and stiff in the orthogonal direction y, keeps the comb-fingers aligned.

The microresonator is a major building block in filters, oscillators [15], and resonant positioning systems [16]. Surface-micromachined microstructures like the microresonator typically range from 0.1 to several μm in thickness and a few hundred μm to a mm in length. Typical space between the microstructure and substrate ranges between 1 and 2 μm.

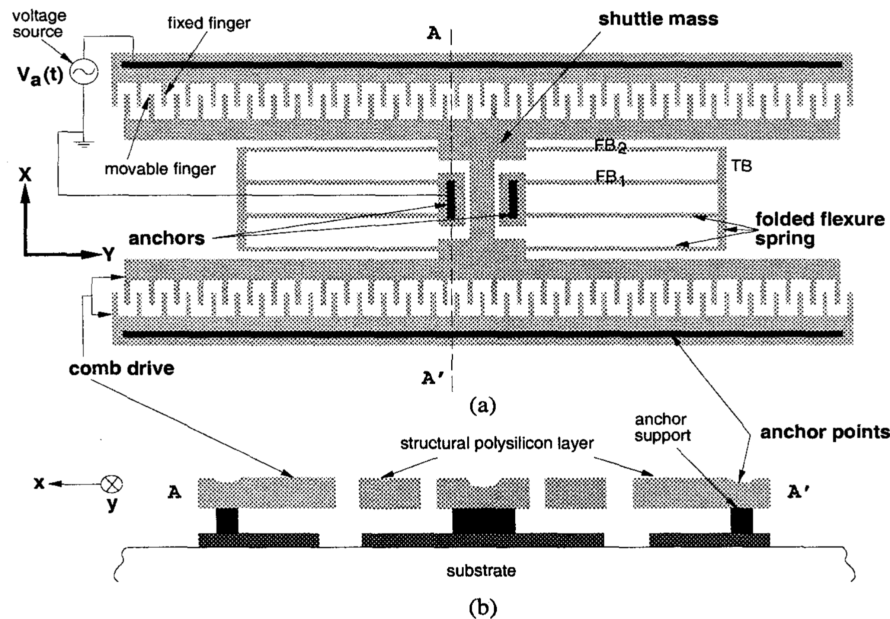

Figure 2: (a) Top-view of the lateral folded-flexure comb-drive microresonator and (b) a simplified device cross-section A-A′ when fabricated using the MUMPS process.

Figure 3 illustrates typical resonator time responses for electrostatic force and x-displacement for a given sinusoidal voltage input assuming air damping is negligible. Note that the force is not centered around zero and has a frequency that is twice that of the applied voltage. Figure 4 shows the typical frequency response of the x-displacement magnitude of a resonator for a sinusoidal input voltage. The response is typical of a second-order linear system. The x-displacement at very-low frequencies is denoted x_0 and x_{max} is the maximum x-displacement that can occur. The frequency corresponding to x_{max} is called the resonant frequency f_x. The ratio x_{max}/x_0 is defined as the quality factor (Q) of the resonator. An alternative definition of the quality factor is $Q = f_x/(f_h - f_l)$, where f_h and f_l are the high and low -3dB points, respectively for the frequency response shown in Figure 4. The major performance specifications of the resonator are f_x, x_{max} and Q. Other performance specifications include f_y (resonant frequency for y-axis motion), f_z (resonant frequency for z-axis motion), and f_θ (resonant frequency for rotation about the z-axis) [14].

2.2 Accelerometer Sensor

Figure 5 shows the topology of a typical accelerometer. Like the resonator, it is composed of beams, plates, anchors, and air-gaps. These primitives make up the major components of the accelerometer which include the U-spring, shuttle, sense comb-drives, and feedback comb-drives. The accelerometer is much more compliant in the x-direction than in the y-direction (note the change in the coordinate system with respect to the resonator). Under the influence of an external acceleration applied in the x-direction, the movable mass experiences an inertial force and undergoes a proportional displacement. Unlike the resonator, the gap between comb-fingers is modulated instead of comb-finger overlap. Accelerometers use finger-gap modulation because sensitivity is much greater, *i.e.*, for the same amount of movement, a greater change in output voltage is produced.

Figure 6 is a simple illustration that shows how shuttle movement in the x-direction is converted to a voltage output. Sensing stems from the parallel-plate capacitors formed from adjacent fixed and movable fingers. Specifically, a voltage is generated by sensing the differential capacitance created by displacement of the movable finger from its nominal position (Figure 6a) to its displaced position (Figure 6b). Before finger movement, the two capacitances C_1 and C_2 are equal. Once the middle finger (MF) moves to the position shown in Figure 6b, C_1 increases and C_2 decreases. So the potential divider output V_o now changes from the nominal value of $V_m/2$, where V_m is the amplitude of the signals applied in opposite phases to the fixed fingers FF_1 and FF_2.

Figure 7 shows plots of an externally applied sinusoidal acceleration and the resulting inertial force and x-displacement. Note that inertial force and acceleration are

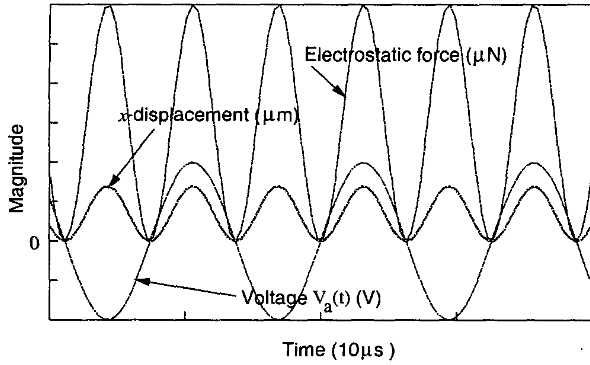

Figure 3: Typical sinusoidal input voltage and resulting electrostatic force and shuttle displacement for a surface-micromachined resonator neglecting damping.

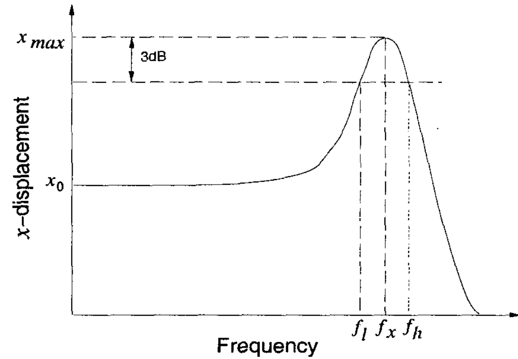

Figure 4: Typical frequency response of x-displacement magnitude for a resonator that is affected by damping.

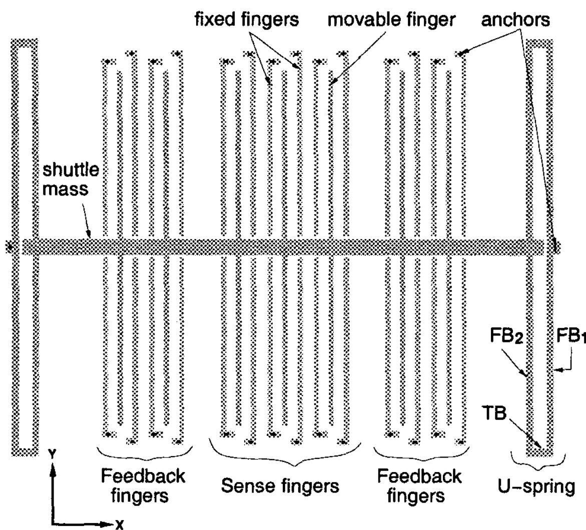

Figure 5: Top-view of a typical accelerometer with the major MEMS components identified.

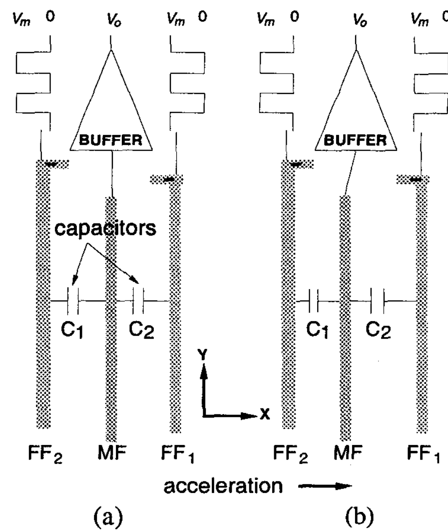

Figure 6: Movement of the middle finger (MF) from (a) its nominal position to (b) its displaced position creates a change in capacitances C_1 and C_2 which is converted to a change in output voltage V_o.

in opposite phase. Similar to the resonator case, these plots were generated ignoring damping. In reality, issues of damping [17], negative spring constant [18], and spring non-linearity [18] complicate accelerometer behavior, discussion of which is beyond the scope of this paper. However, the non-linear behavior exhibited by an accelerometer is prominent for displacements greater than five percent of comb-finger gap, which is a level outside the normal operating range.

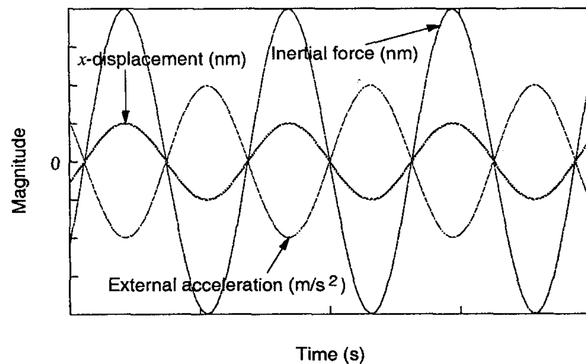

Figure 7: Sinusoidal acceleration input and resulting inertial force and shuttle displacement for a typical surface-micromachined accelerometer assuming negligible damping.

2.3 MEMS Failure Sources

The performance of MEMS devices can be affected by a variety of failure sources. Sources include but are not limited to:

1. *Stiction* is the adhesion of the microstructure to adjacent surfaces. The large surface area and small offset from adjacent surfaces make microstructures like the resonator and the accelerometer vulnerable to stiction. It can occur during the final steps of the micromachining process (when the structure is released) or after packaging of the device due to out-of-range input signals or electromechanical instability [19].
2. *Curvature* is another result of manufacturing conditions that cause structures of the micromechanical device to curl or buckle out of plane.
3. *Particulate contaminations* can occur in fabrication [10] and assembly. Spot defects resulting from particulates can cause a significant perturbation in the structural and material properties of the microstructure [8].
4. *Etch variations* lead to over-etch or under-etch of the device layers thus changing the width and length of device components.

Besides the above-mentioned failure sources, there are other unlikely sources such as *package tilt* and *side-wall angle* [20]. Package tilt is caused by incorrect packaging that causes the plane of the MEMS device to be non-horizontal. Side-wall angle is non-vertical side-walls. Both package tilt and asymmetric side-wall angles can lead to cross-axis coupling, *i.e.*, sensitivity to inputs in directions orthogonal to the sense direction.

We consider three of most likely failure sources, namely, stiction, dielectric particles, and etch variations. The effects of each failure source and that of particles and etch variations in combination, on a resonator and an accelerometer, are studied. Specifically, the impact on resonant frequency f_x is examined in detail. A typical acceptable performance range for f_x is a frequency band of $0.5f_x$ centered around the nominal f_x value. This range is based on the capability of the calibration procedure to "pull" the device performance to within the user-defined specification.

3 Resonator Analysis

A folded-flexure resonator design was synthesized using the MEMS synthesis tool of [14] with the following objectives: $f_x = 100$ kHz, $x_{max} = 2\mu$m, and $Q > 5$. The typical topology of a folded-flexure resonator is shown in Figure 2a.

Three major sources of failures are considered, namely vertical stiction, particles and etch variations. Mechanical FEA is used to analyze the impact of defects caused by the failure sources on the x-resonant frequency f_x. For this resonator, the acceptable performance range for f_x lies in the range [75 kHz, 125 kHz].

3.1 Finger Stiction

Even a single movable finger stuck down to the substrate for a resonator is catastrophic. A stuck movable finger causes the displacement in the x-direction to be less than 15% of its nominal value. Movement is hindered because the fingers, which are much longer along the x-axis as compared to the y-axis (Figure 2a), have high resistance to compression or extension in the x-direction. For a single stuck finger, the spring constant k_x increases by more than 500% over its nominal value.

3.2 Etch Variation

Etch variation is the difference between the nominal etch and the actual etch of the device and can be either positive

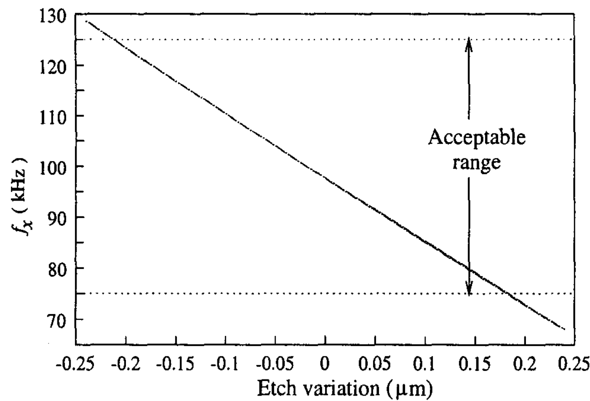

Figure 8: Change of x-resonant frequency f_x for the resonator with etch variation.

(over-etch) or negative (under-etch). Consider a rectangular structure with nominal length l, width w, and thickness t. Over-etch of amount Δ decreases length and width to $l - 2\Delta$ and $w - 2\Delta$, respectively. Similarly, under-etch of amount Δ increases length and width to $l + 2\Delta$ and $w + 2\Delta$, respectively. Note that the structure thickness t remains unchanged by etch variation. Local etch variation from one device region to another is considered negligible due to the small area of the device. Etch-loading effects, such as different etch values for different regions of the device, have been ignored since real-life designs introduce additional features (which do not affect FEA results) to eliminate them. The amount of etch variation was varied in the range of [-0.24 μm, +0.24 μm] and the corresponding models generated for mechanical FEA were altered accordingly. The etch variation range used is based on typical values found in an industrial fabrication process.

Figure 8 shows that f_x (as obtained by FEA) varies almost linearly with respect to the amount of etch variation. The resulting range of f_x is [68 kHz, 129 kHz] with 98 kHz corresponding to no over/under etch. Thus, for this resonator design, it is possible for etch variation alone to cause unacceptable behavior.

3.3 Particle Contaminations

In prior work, we have analyzed the impact of particulates on resonator designs using three-dimensional FEA [21]. Analysis of the FEA results has led to defect classification based on resonant frequency deviation [8] and designs that are less susceptible to particulate defects [7]. Here, we choose to target particulate defects whose behavior is difficult to detect. Catastrophic defects due to particles between fixed and movable fingers, and the shuttle mass and the substrate, are therefore not considered.

The symmetry of the resonator layout with respect to the x and y axes (Figure 2a) can be used to reduce the area of particle injection to just one quadrant. We consider the impact of particles alone as well as the effect of both particles and etch variation to analyze the combined effect of the two failure sources on the resonator.

Figure 9 shows the variation of the resonant frequency f_x for particles located at various positions underneath flexure beam FB_1 (see Figure 2a). A particle located under a beam behaves as an extra, unwanted anchor to the substrate. The location of the particle under FB_1 is expressed as a percentage of beam length with the terminal anchor serving as the 0% point and the FB_1-TB (truss beam) intersection corresponding to the 100% mark. The resonant frequency ranges of [129.0 kHz, 153.0 kHz], [123.0 kHz, 147.0 kHz], [110.0 kHz, 132.0 kHz], [98.0 kHz, 117.0 kHz], [85.0 kHz, 102.0 kHz], [73.0 kHz, 88.0 kHz], and [68.0 kHz, 82.0 kHz] result for etch variation values of -0.24, -0.2, -0.1, 0, 0.1, 0.2 and 0.24 μm, respectively. Thus, an FB_1 anchor defect combined with an over-etch of 0.1 μm or less does not cause failure; however, other combinations may.

Figure 10 is similar to Figure 9 except that it shows the variation of f_x for particles located at various positions underneath flexure beam FB_2 (see Figure 2a). The location of the particle is expressed as a percentage of the beam length with the FB_2-TB intersection serving as the 0% point and the FB_2-shuttle mass intersection corresponding to the 100% mark. For FB_2 anchor defects, the resonant frequency ranges of [155.0 kHz, 228.0 kHz], [149.0 kHz, 221.0 kHz], [134.0 kHz, 202.0 kHz], [118.0 kHz, 181.0 kHz], [103.0 kHz, 162.0 kHz], [89.0 kHz, 142.0 kHz], and [83.0 kHz, 135.0 kHz] result for etch variation values of -0.24, -0.2, -0.1, 0, 0.1, 0.2 and 0.24 μm, respectively. Thus, an FB_2 anchor defect combined with any amount of under-etch always causes failure. However, combinations that include over-etch may or may not cause failure.

We have considered only one representative location underneath TB (see Figure 2a) since its rigidity in the x direction ensures that all points on TB have essentially the same x-displacement. This implies that anchor defects along TB all have virtually the same impact on behavior. For example, an anchor defect under the center of TB gives f_x = 154.0 kHz, 148.0 kHz, 133.0 kHz, 117.5 kHz, 102.5 kHz, 88.5 kHz, and 82.5 kHz for etch variation values of -0.24, -0.2, -0.1, 0, 0.1, 0.2, and 0.24 μm, respectively. Similar to FB_2 anchor defects, any amount of under-etch combined with a TB anchor defect causes failure. However, combinations with over-etch cannot push f_x outside the acceptable range.

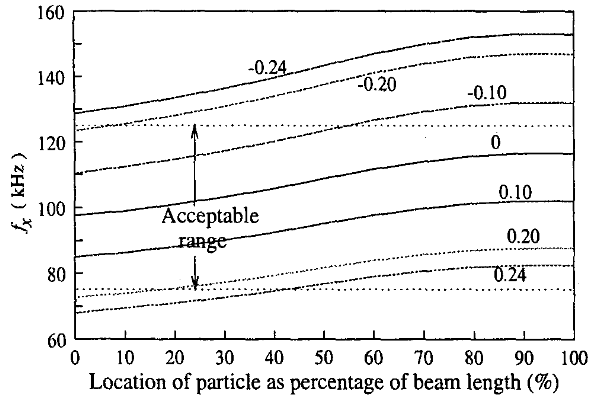

Figure 9: Variation of the x-resonant frequency f_x for an anchor defect located under flexure beam FB_1 of the resonator for etch variation values in the range of $[-0.24\mu m, 0.24\mu m]$.

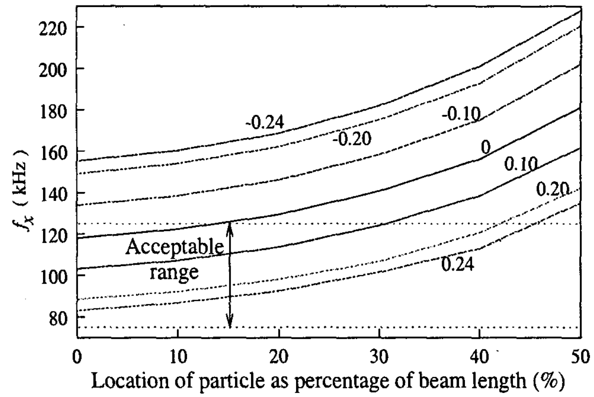

Figure 10: Variation of the x-resonant frequency f_x for an anchor defect located under flexure beam FB_2 of the resonator for etch variation values in the range of $[-0.24\mu m, 0.24\mu m]$.

Defect type	**Etch variation values (μm)**							
	-0.24	**-0.20**	**-0.10**	**0**	**0.10**	**0.20**	**0.24**	**-0.24 – 0.24**
None	129.0	123.0	110.0	98.0	85.0	73.0	68.0	[68.0, 129.0]
FB_1 anchor	[129.0, 153.0]	[123.0, 147.0]	[110.0, 132.0]	[98.0, 117.0]	[85.0, 102.0]	[73.0, 88.0]	[68.0, 82.0]	[68.0,153.0]
FB_2 anchor	[155.0, 228.0]	[149.0, 221.0]	[134.0, 202.0]	[118.0, 181.0]	[103.0, 162.0]	[89.0, 142.0]	[83.0, 135.0]	[83.0, 228.0]
TB anchor	154.0	148.0	133.0	117.5	102.5	88.5	82.5	[82.5, 154.0]
Finger stiction	-	-	-	$\gg 98.0$	-	-	-	-

Table 1: Resonant frequency ranges, expressed in kHz, corresponding to different defect types for the resonator, listed for the full etch variation range of $[-0.24\mu m, 0.24\mu m]$.

3.4 Discussion

Table 1 summarizes the simulation results for the resonator. Specifically, row 1 of Table 1 lists the change in resonant frequency f_x for specific values of over- and under-etch and for the entire range of etch variation values. Rows 2–4 list the resulting f_x ranges for various combinations of etch variation and anchor defects under the flexure and truss beams. From Table 1, it is easy to identify examples of behavior overlap, masking, and construction.

Recall that the acceptable range for f_x lies in [75 kHz, 125 kHz]. Table 1 indicates that all the failure sources (except stiction) considered for the resonator have behavior that overlaps that of an acceptable design. Thus, it is possible that a defective device may go undetected if only an f_x measurement is performed. Behavior overlap also exists among the failure sources. The last column of Table 1 shows that all the behaviors overlap with the likely range of etch variation.

Examining the data more closely, we can illustrate cases of misbehavior masking. For example, Figure 9 shows that an over-etch of 0.2 μm alone causes the device to fail but when combined with an anchor defect located at the 30% point of the beam FB_1, f_x falls within the acceptable range. This is expected since over-etch and FB_1 anchor defects change f_x in opposing directions. Masking is also possible for etch variation and FB_2 anchor defects. Figure 10 shows that an anchor defect located at the 20% point of FB_2 causes failure; however, when combined with an over-etch of 0.1 μm, f_x falls within the acceptable range.

Finally, cases of misbehavior construction can be identified. An FB_1 anchor defect in the presence of an over-etch can cause a significant increase in resonant frequency. For example, Figure 9 shows that an over-etch of 0.1 μm combined with an anchor defect located at the 90% point of FB_1 increases f_x to approximately 132 kHz, which is well outside the acceptable range of [75 kHz, 125 kHz]. However, as indicated in Table 1, neither one alone pushes f_x outside the acceptable range.

4 Accelerometer Analysis

An accelerometer design was synthesized using a synthesis tool similar to that of [22]. The constraints for synthesis are minimum area and minimum noise. The desired sensitivity is 5 mV/G and the full-scale input range is 50G, where G is the acceleration due to gravity. The typical topology of

an accelerometer is shown in Figure 5. The effect of vertical stiction on the movable fingers, etch variation, and particles on the accelerometer's x-resonant frequency f_x are analyzed. For this accelerometer, the nominal value of f_x is 5.23 kHz and the acceptable performance range for f_x lies in the range [3.92 kHz, 6.54 kHz].

4.1 Vertical Stiction of Fingers

Figure 11 shows the variation of f_x with the number of movable fingers (shown as MF in Figure 6) stuck down on the substrate. The finger tip is the most vulnerable point for vertical stiction since the force required to make it contact the substrate is minimum at this location. Hence, we have considered stiction at the tips alone. For only one stuck finger, f_x becomes approximately 8.8 kHz, which is catastrophic. Vertical stiction of movable fingers therefore leads to an easily detectable failure for this particular accelerometer topology.

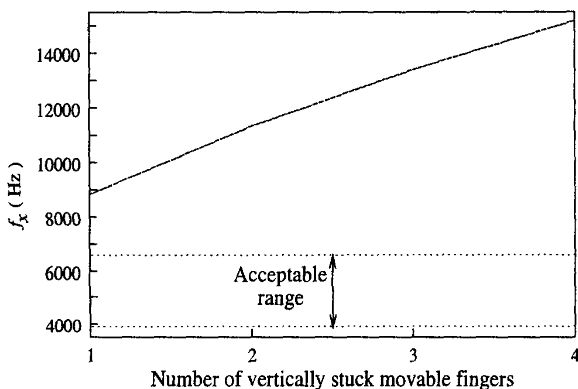

Figure 11: Variation of x-resonant frequency f_x for the accelerometer with a varying number of movable fingers stuck down.

4.2 Etch Variation

As in the case of the resonator, the etch variation range of [-0.24 μm, +0.24 μm] is used and the sign convention for etch variation is the same: over-etch is positive and under-etch is negative. Figure 12 shows the variation of f_x (as obtained by FEA) for our accelerometer design to be almost linear with the amount of etch variation. The resulting range of f_x is [4.17 kHz, 6.30 kHz] with 5.23 kHz corresponding to zero etch variation, *i.e.*, the x-resonant frequency of the nominal design. Thus, it is unlikely that etch variation alone can cause misbehavior of this particular accelerometer.

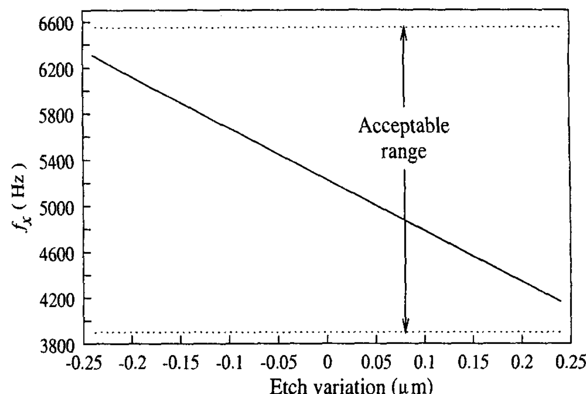

Figure 12: Variation of x-resonant frequency f_x for the accelerometer with etch variation.

4.3 Particle Contaminations

As in the case of the resonator, we have used the symmetry of the accelerometer topology (Figure 5) to limit the area of particle injection to just one quadrant. As shown in Figure 5, the flexure beam FB_1 connects the truss beam (TB) and the anchor, while FB_2 connects TB and the shuttle mass. The movement of FB_2 is always more than that of FB_1 during device operation. Hence a particle on the FB_2 is expected to be more harmful than an identical particle on FB_1.

Figure 13 shows the variation of f_x with particles located under flexure beam FB_1. The location of the anchor defect is based on a percentage of the beam length with the FB_1 beam anchor marking the 0% point and the 100% point corresponding to where FB_1 meets the truss beam TB. For FB_1 anchor defects, the resonant frequency ranges for etch variation values of -0.24, -0.2, -0.1, 0, 0.1, 0.2 and 0.24 μm are [6.30 kHz, 6.76 kHz], [6.12 kHz, 6.57 kHz], [5.67 kHz, 6.11 kHz], [5.23 kHz, 5.65 kHz], [4.78 kHz, 5.18 kHz], [4.34 kHz, 4.72 kHz], and [4.17 kHz, 4.54 kHz], respectively. Thus, an FB_1 anchor defect combined with any value of over-etch or any value of etch variation greater than -0.1 μm does not cause failure; however, other combinations may.

Figure 14 is similar to Figure 13 except that it shows the variation of f_x with particles located under flexure beam FB_2. The location of the anchor defect is based on a percentage of the beam length with the FB_2-TB joint marking the 0% point and the 100% point corresponding to where FB_2 meets the shuttle mass. For FB_2 anchor defects, the resonant frequency ranges are [6.96 kHz, 11.24 kHz], [6.78 kHz, 11.00 kHz], [6.28 kHz, 10.36 kHz], [5.80 kHz, 9.72 kHz], [5.32 kHz, 9.06 kHz], [4.84 kHz, 8.38 kHz], and [4.65 kHz,

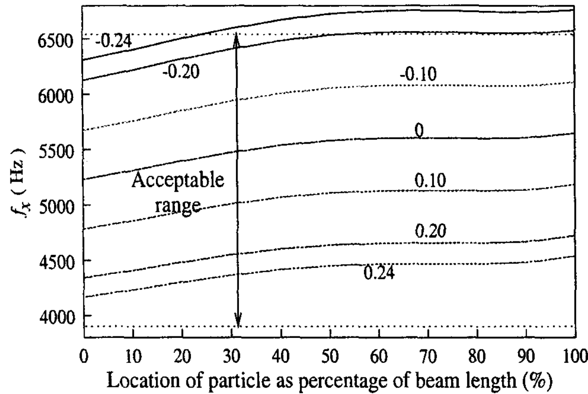

Figure 13: Variation of the x-resonant frequency f_x for an anchor defect located under flexure beam FB_1 of the accelerometer for etch variation values in the range of $[-0.24\mu m, 0.24\mu m]$.

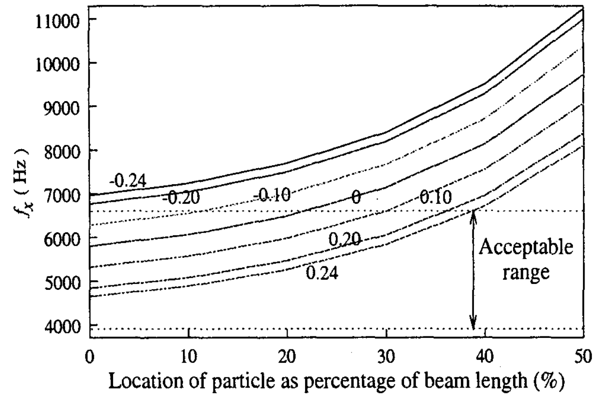

Figure 14: Variation of the x-resonant frequency f_x for an anchor defect located under flexure beam FB_2 of the accelerometer for etch variation values in the range of $[-0.24\mu m, 0.24\mu m]$.

8.10 kHz] for etch variation values of -0.24, -0.2, -0.1, 0, 0.1, 0.2 and 0.24 μm, respectively. Thus, an FB_2 anchor defect combined with an under-etch of more than 0.2 μm always causes failure. However, combinations that include over-etch and other values of under-etch may or may not cause failure.

Figure 15 shows the variation of f_x for anchored particles under movable fingers. The 0% point marks the movable finger tip and the 100% point corresponds to the movable finger base where it joins the shuttle mass. For this defect type the resonant frequency ranges are [8.40 kHz, 11.07 kHz], [8.22 kHz, 10.89 kHz], [7.76 kHz, 10.43 kHz], [7.31 kHz, 9.98 kHz], [6.72 kHz, 9.53 kHz], [6.23 kHz, 9.09 kHz], and [6.03 kHz, 8.91 kHz] for etch variation values of -0.24, -0.2, -0.1, 0, 0.1, 0.2 and 0.24 μm, respectively. These results indicate that any amount of under-etch combined with a movable finger anchor defect causes failure. However, finger defects with over-etch values of more than 0.2 μm may or may not cause failure.

Figure 16 gives the variation of f_x for particles attached between movable and fixed fingers. The 0% point marks the movable finger tip and the 100% point corresponds to the movable finger base. The resonant frequency ranges are [8.28 kHz, 9.78 kHz], [8.07 kHz, 9.56 kHz], [7.57 kHz, 9.00 kHz], [6.65 kHz, 8.44 kHz], [6.15 kHz, 7.89 kHz], [5.74 kHz, 7.34 kHz], and [5.50 kHz, 7.13 kHz] for etch variation values of -0.24, -0.2, -0.1, 0, 0.1, 0.2 and 0.24 μm, respectively. These plots are unique in their shape, in that, each has a peak. Similar to movable finger anchor defects, any amount of under-etch combined with an inter-finger defect causes failure. However, combinations with over-etch values may or may not push f_x outside the acceptable range.

Particles located between/under fingers of the accelerometer are in sharp contrast to corresponding cases for the resonator since in the latter, this type of defects always result in catastrophic behavior; however, for the accelerometer some of these cases are within the acceptable range.

4.4 Discussion

Similar to Table 1, Table 2 summarizes the simulation results for the accelerometer from which many examples of behavior overlap, dominance, construction, and masking can be identified.

Like the resonator, the f_x ranges due to etch variation, particles, and combinations thereof all overlap with the acceptable f_x range of [3.92 kHz, 6.54 kHz]. Again, like the resonator, there is one exception involving stiction. From Table 2, we can see that the change in f_x due to one or more stuck fingers is well outside the acceptable range.

Other behavior relationships include:

- **Construction:** Behavior construction occurs for an FB_1 anchor defect combined with under-etch. As shown in Figure 13, an under-etch of 0.24 μm combined with an anchor defect located at 50% point of beam FB_1 pushes f_x outside the acceptable range, while separately they do not. Another example involves an FB_2 anchor defect and under-etch. In particular, Figure 14 shows that an under-etch of 0.1 μm combined with an anchor defect located at the 20% point of beam FB_2 cause failure, but are acceptable when existing individually.
- **Masking:** Behavior masking occurs for FB_2 anchor

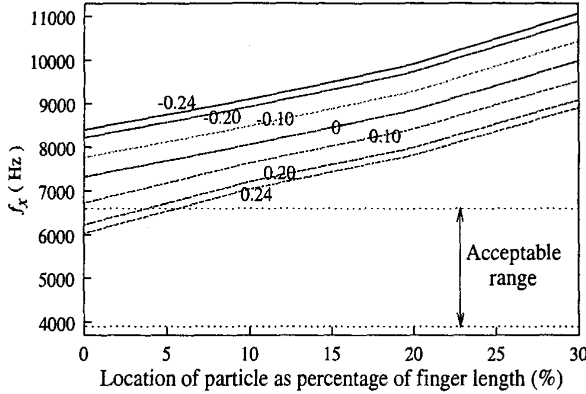

Figure 15: Variation of the x-resonant frequency f_x for different locations of a particle anchored under a movable finger of the accelerometer for etch variation values in the range of $[-0.24\mu m, 0.24\mu m]$.

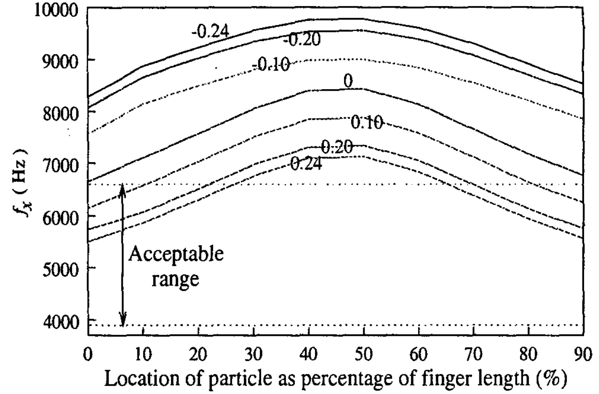

Figure 16: Variation of the x-resonant frequency f_x for different positions of a particle welded between movable and fixed fingers of the accelerometer for etch variation values in the range of $[-0.24\mu m, 0.24\mu m]$.

Defect type	Etch variation values (μm)							
	-0.24	**-0.20**	**-0.10**	**0**	**0.10**	**0.20**	**0.24**	**-0.24 – 0.24**
None	6.30	6.12	5.67	5.23	4.78	4.34	4.17	[4.17, 6.30]
FB_1 anchor	[6.30, 6.76]	[6.12, 6.57]	[5.67, 6.11]	[5.23, 5.65]	[4.78, 5.18]	[4.34, 4.72]	[4.17, 4.54]	[4.17, 6.76]
FB_2 anchor	[6.96, 11.24]	[6.78, 11.00]	[6.28, 10.36]	[5.80, 9.72]	[5.32, 9.06]	[4.84, 8.38]	[4.65, 8.10]	[4.65, 11.24]
Movable finger anchor	[8.40, 11.07]	[8.22, 10.89]	[7.76, 10.43]	[7.31, 9.98]	[6.72, 9.53]	[6.23, 9.09]	[6.03, 8.91]	[6.03, 11.07]
Welded fingers	[8.28, 9.78]	[8.07, 9.56]	[7.57, 9.00]	[6.65, 8.44]	[6.15, 7.89]	[5.74, 7.34]	[5.50, 7.13]	[5.50, 9.78]
Movable finger stiction	-	-	-	[8.83, 15.18]	-	-	-	-

Table 2: Resonant frequency ranges, expressed in kHz, corresponding to different defect types for the accelerometer, listed for the full etch variation range of $[-0.24\mu m, 0.24\mu m]$.

defects and etch variation. Figure 14 shows that the effect of an anchor defect located at the 15% point of beam FB_2 is virtually negated by an over-etch of 0.2 μm.

- **Dominance:** Behavior dominance is illustrated for FB_2 anchor defects and particles welded between fixed and movable fingers. Specifically, FB_2 anchor defects dominate welded-finger defects since the f_x range for the former ([4.65 kHz, 11.24 kHz]) includes the latter ([6.03 kHz, 11.07 kHz]).

5 Conclusions

We have analyzed the effects of defects caused by three major failure sources—vertical stiction, foreign particles, and etch variations—on the resonant frequency of a surface-micromachined resonator and accelerometer. For the design topologies considered, it was shown that a single stuck finger due to stiction always has a catastrophic impact on resonant frequency. However, for particles, etch variation, and the combination of the two, there were instances of defects where resonant frequency remained within the acceptable range. Thus, indicating (as expected) that resonant frequency test is not sufficient for detecting all defects from the failure sources considered. Other specification-based tests can and should be used.

The relationships among behaviors resulting from the failure sources also have been examined. Similar to digital and analog electronics test, examples of behavior overlap, dominance, construction and masking were observed. Understanding these relationships is important for a variety of reasons. For MEMS manufacturing test, overlap and dominance is key for developing efficient tests but hinders failure analysis since similar behaviors can point to a variety of failure sources. Understanding behavior masking and construction is also important because of the implications on quality and long-term reliability.

Our future work in this area includes the analysis of other failure sources such as side-wall angle, device curvature, and package tilt. Both the mechanical and electrical effects of these failure sources, in isolation and in various

combinations, will be examined to construct comprehensive fault models for MEMS. In addition, the criteria for misbehavior classification will be broadened to include other performance specifications such as dc-offset, linearity, sensitivity, and cross-axis sensitivity.

References

[1] T. Mukherjee, G. K. Fedder and R. D. Blanton, "Hierarchical Design and Test of Integrated Microsystems," *IEEE Design and Test of Computers*, pp. 18-27, Oct.-Dec. 1999.

[2] L. J. Hornbeck, "Digital Light Processing update: status and future applications," *Proc. of the SPIE - The International Society for Optical Engineering*, Vol. 3634, pp. 158-170, Jan. 1999.

[3] R. S. Payne, S. Sherman, S. Lewis and R. T. Howe, "Surface Micromachining: From Vision to Reality to Vision (accelerometer)," *Proc. of International Solid State Circuits Conference*, pp. 164-165, Feb. 1995.

[4] D. A. Koester, R. Mahadevan and K. W. Markus, *MUMPS Introduction and Design Rules*, MCNC MEMS Technology Applications Center, 3021 Cornwallis Road, Research Triangle Park, NC, Oct. 1994.

[5] B. Charlot, S. Mir, E. F. Cota, M. Lubaszewski and B. Courtois, "Fault Simulation of MEMS Using HDLs," *Symposium on Design Test and Microfabrication of MEMS/MOEMS*, pp. 70-77, March 1999.

[6] B. Charlot, S. Moussouris, S. Mir and B. Courtois, "Fault Modeling of Electrostatic Comb-drives for MEMS," *Proc. of International Test Conference*, pp. 398-405, Sept. 1999.

[7] N. Deb, S. V. Iyer, T. Mukherjee and R. D. Blanton, "MEMS Resonator Synthesis for Defect Reduction," To appear in *Journal of Modeling and Simulation of Microsystems*.

[8] T. Jiang and R. D. Blanton, "Particulate Failures for Surface-Micromachined MEMS," *Proc. of International Test Conference*, pp. 329-337, Sept. 1999.

[9] A. Castillejo, D. Veychard, S. Mir, J. M. Karam and B. Courtois, "Failure Mechanisms and Fault Classes for CMOS-Compatible Microelectromechanical Systems," *Proc. of International Test Conference*, pp. 541-550, Sept. 1998.

[10] A. Kolpekwar, R. D. Blanton and D. Woodilla, "Failure Modes for Stiction in Surface-Micromachined MEMS," *Proc. of International Test Conference*, pp. 551-556, Oct. 1998.

[11] W. C. Tang, T.-C. H. Nguyen, M. W. Judy, and R. T. Howe, "Electrostatic Comb Drive of Lateral Polysilicon Resonators," *Sensors and Actuators A*, Vol. 21, Nos. 1-3, pp. 328-331, Feb. 1990.

[12] http://www.mdl.sandia.gov/micromachine/technologies.html

[13] http://mems.mcnc.org/imems/tech.html

[14] T. Mukherjee, S. Iyer and G. K. Fedder, "Optimization-based Synthesis of Microresonators," *Sensors and Actuators A*, Vol. 70, Nos. 1-2, pp. 118-127, Oct. 1998.

[15] R. T. Howe and C. T.-C. Nguyen, "Micromechanical Resonators for Frequency References and Signal Processing," *Proc. of International Electron Devices Meeting*, p. 343, Dec. 1994.

[16] M.-H. Kiang, O. Salgaard, K. Y. Lau and R. S. Muller, "Electrostatic Combdrive-Actuated Micromirrors for Laser-Beam Scanning and Positioning," *Journal of Microelectromechanical Systems*, Vol. 7, No. 1, pp. 27-37, March 1998.

[17] T. Veijola, H. Kuisma and J. Lahdenpera, "The Influence of Gas-Surface Interaction on Gas Film Damping in a Silicon Accelerometer," *Sensors and Actuators A*, Vol. 66, Nos. 1-3, pp. 83-92, April 1998.

[18] G. K. Fedder, *Simulation of Microelectromechanical Systems*, Ph.D. thesis, University of California at Berkeley, Sept. 1994.

[19] R. Maboudian and R.T. Howe, "Critical Review: Adhesion in Surface Micromechanical Structures," *Journal of Vacuum Science and Technology B*, Vol. 15, No. 1, pp. 1-20, Jan. 1997.

[20] N. R. Swart, "A Design Flow for Micromachined Electromechanical Systems," *IEEE Design and Test of Computers*, pp. 39-47, Oct.-Dec. 1999.

[21] A. Kolpekwar, C. Kellen and R. D. Blanton, "MEMS Fault Model Generation using CARAMEL," *Proc. of International Test Conference*, pp. 557-566, Oct. 1998.

[22] T. Mukherjee, Y. Zhou and G. K. Fedder, "Automated Optimal Synthesis of Microaccelerometers," *Proc. of IEEE International Micro Electro Mechanical Systems Conference*, pp. 326-331, Jan. 1999.